18TH WORLD CONFERENCE ON EARTHQUAKE ENGINEERING
WCEE2024
MILAN

MILAN, ITALY
30TH JUNE - 5TH JULY 2024
www.wcee2024.it

PREDICTING TSUNAMI INUNDATION AND IMPACTS USING OFFSHORE WAVE DATA AND ML FOR RAPID ASSESSMENT

N. Ragu Ramalingam[1,5], A. Rao[2], A. Abbate[3,4], E. Briseid Storrøsten[5], K. Johnson[2], G. Davies[6], F. Løvholt[5], S. Lorito[4], M. Pagani[2], M. Martina[1]

University School for Advanced Studies (IUSS Pavia), Pavia, Italy, naveen.raguramalingam@iusspavia.it

[2] Global Earthquake Model Foundation, Pavia, Italy

[3] University of Trieste, Department of Mathematics and Geosciences, Trieste, Italy

[4] Istituto Nazionale di Geofisica e Vulcanologia, Rome, Italy

[5] Norwegian Geotechnical Institute, Oslo, Norway

[6] Geoscience Australia, Canberra, Australia

Abstract: *In the aftermath of a tsunami event, accurate and timely information on inundation and its impacts is crucial for effective emergency response and recovery efforts. Current methods employ remote sensing data from satellite imagery or aerial photography for inundation mapping and damage assessment. This approach often faces constraints of acquisition time and coverage. Alternatively, urgent computing can be used for tsunami forward modelling and risk assessment once sufficient information about the tsunami earthquake source and offshore observations are available. This may require priority access to a high-performance computing facility when large areas at high resolution need to be assessed, which may not be possible in many regions at risk of a tsunami. This research suggests the use of offshore tsunami wave time series, which can be derived from offshore tsunami sensors or low-fidelity tsunami propagation models run in real-time, as input to a machine learning (ML) based surrogate. The ML surrogate provides a rapid prediction of the tsunami inundation that can be used to calculate the impact onshore in terms of the population affected and building damage loss. The ML based surrogate is made of a neural network model that was trained using a large number of synthetic tsunami events. This training dataset provides details on offshore tsunami waveforms and their associated onshore flooding hazards. Such a quick prediction tool can help in modelling many different scenarios due to the uncertainty in the characterization of the earthquake source in the early stages post a tsunami event, providing real-time probabilistic estimates of the unknown tsunami impacts. We illustrate an application of the described methodology to the eastern coast of Sicily.*

1 Introduction

In the wake of a tsunami, rapid assessment of the hazard and impact of the event in terms of the inundation and damage onshore can assist in timely emergency response, management and recovery initiatives. Typically, post-event hazard and damage assessment rely on field surveys (Mori et al., 2011; Fraser et al.,

2013) and remotely sensed imagery data from satellite or drone imagery (Bai et al., 2018; Ahmed and Güneyli, 2023). When sufficient information about the earthquake source is available, full forward tsunami modelling can also be performed to assess inundation and impact at high resolution but relies on the availability of priority access to urgent computing (Kosaka et al., 2023, Folch et al. 2023). A feasible alternative is to use offshore and coastal tsunami monitoring networks that provide a direct mechanism for monitoring earthquakes and tsunamis. Tsunami early warning and mitigation systems by the Tsunami Service Providers (TSPs) covering many of the seas worldwide have been established under the IOC-UNESCO framework like NEAMTWS (UNESCO 2007) for the North-eastern Atlantic, the Mediterranean and connected seas. Other examples and regional initiatives have been discussed by Igarashi et al. (2016) and Mulia and Satake (2020). Several statistical, algorithmic and machine learning based approaches exist that can be used to predict the tsunami waveforms, inundation time series and maxima based on the inputs from such observation systems and available precomputed tsunami propagation and inundation databases (Titov et al., 2005, Baba et al., 2014, Gusman et al., 2014, Makinoshima et al., 2021, Mulia et al., 2022)**.**

For many regions at risk of tsunami, such observation systems are either not yet available or unfeasible to deploy due to their cost and technical constraints. In such situations, a possible strategy is to combine early earthquake source information with numerical modelling of tsunami waveforms offshore. Then, using an ML surrogate for predefined locations along a coastal region we can predict the tsunami inundation, similar to the approach of Gusman et al. (2014) and Núñez et al. (2022). In this study, we employ a neural network architecture called the Encoder-Decoder model for the prediction of the tsunami maximum flood depth over a large number of locations in Catania, Sicily region of Italy. Synthetic tsunami waveforms and inundation depths from hypothetical events are used to train and test the model. Further, the inundation predictions from the model are combined with the exposure information in the form of the population count and built-up area to provide detailed insight into the tsunami impact and evaluate its reliability for decision making in the proposed rapid assessment application.

2 Data and methods

2.1 Tsunami data

The tsunami data used in this study focuses on the Italian city of Catania, located on Sicily's east coast, and considers tsunamis generated by submarine earthquakes along the Hellenic subduction zone (HSZ). A total of 23,086 synthetic events, based on the hazard disaggregation from the NEAMTHM18 Tsunami Hazard Model (Basili et al., 2021), are included in our dataset for HSZ. The tsunami waveforms and local high-resolution inundation for the region of Catania were modelled by Gibbons et al. (2020) using stochastic heterogeneous slip for each event. These computations were carried out using the Tsunami-HySEA implementation of the non-linear shallow water equation (de la Asunción et al., 2013) and executed on Tier0 high performance computers under the ChEESE project (Folch et al., 2023).

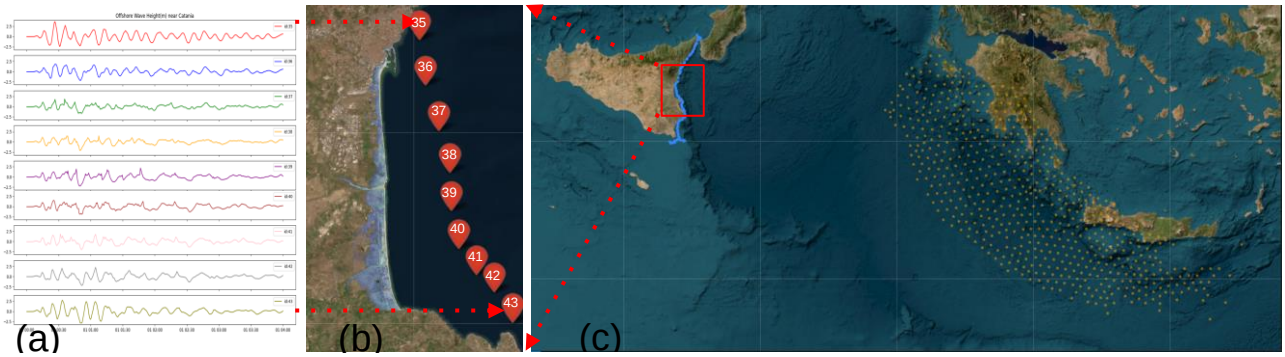

Figure 1. Tsunami data for the region of Catania: (a) Example of tsunami waveforms of 4 hours as 480 data points for the nine offshore locations at 50-m depth marked in panel (b), (b) Example of maximum flood depth recorded across a ~10 m mesh of dimensions 912 x 2224 and (c) Earthquake epicentres from the Hellenic subduction zone (HSZ) at which tsunami is modelled in the dataset is shown in orange and offshore locations in blue.

The tsunami waveforms at nine offshore locations #35-43(Fig. 1b) along the 50 m isobath from these simulations are used as the inputs for the ML surrogate. At such depths, low-fidelity linear shallow water modelling can often provide sufficiently accurate results as done by Molinari et al. (2016) in this region. The inundation in these simulations is modelled using a nested grid approach where the final onshore inundation is modelled at approximately 10 m resolution in the geographic coordinate system. Each simulation is run for a duration of 4 hours from the initiation of the earthquake. Figures 1 and 3 provide an overview of the tsunami data, modelling location and the summary statistics of the tsunami data.

2.2 The Encoder–Decoder model

The structure of the model consists of three main components: an encoder, latent variables and a decoder. Here the function of an encoder f is to map a given input x to a reduced number of latent variables z and the decoder g to map the latent variables back to a high dimensional reconstruction r of the input x using w and b the learned weights and biases.

$$z = f(x, w, b) \quad (1)$$

$$r = g(z, w, b) \quad (2)$$

The model is chosen for its ability to encode the most important features of the input (i.e., the offshore tsunami waveform) to the latent variables and decode it to the maximum inundation depth at locations onshore. Similar model structures have been used in the field of tsunami prediction but for its denoising or filling property (Liu et al., 2021; Wang et al., 2023) where a limited sequence of the offshore tsunami waveform was used as input to predict the complete tsunami waveform at coastal locations. In our case we would like to use the model for feature translation, utilising the complete sequence of the available waveform. We use convolutional neural network (CNN) layers as the encoder to map them to the reduced latent variable and use a fully connected neural network for the decoding to the maximum inundation depth. The final structure of the model and its individual components are depicted in Figure 2.

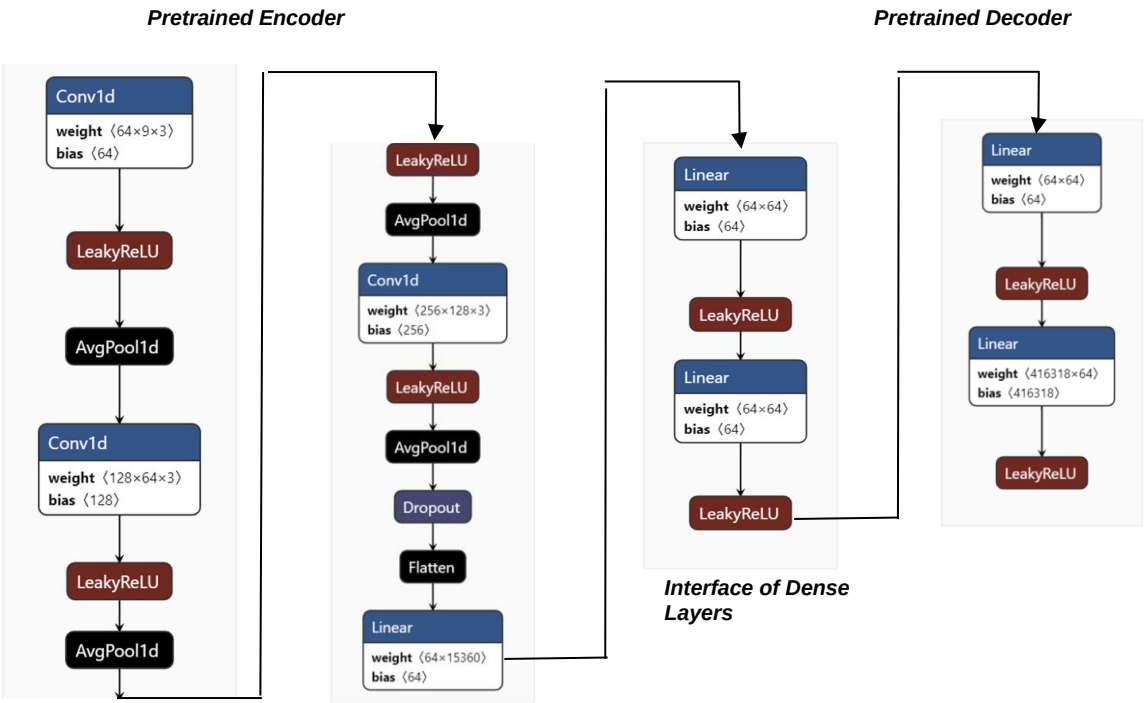

Figure 2. Encoder-Decoder model architecture implemented in the PyTorch framework

2.3 Pretraining, finetuning and testing

To capture the required representation of the overall dataset in the training set, we first select a random half of our dataset. Then, within this subset, we divide the data into 80 evenly spaced interval bins based on the absolute maximum wave amplitude value of each event at location 41. This site was also used in hazard disaggregation by Basili et al. (2021). These bins cover a range from 0 to 2.5 m, with the last bin spanning from 2.5 m to the maximum value observed at location 41. In each of these bins, we select 40 events. We further constrain the selection with a threshold of 0.1 m for the maximum wave amplitude and 0.2 m for the maximum inundation depth, as smaller events than these would not be significant for our application. This leads to a final selection of 2586 events from the overall dataset of 23086, shown in Figure 3. This selection was divided with a 75:25 split into 1,939 events for training the model, 647 events to validate/check for overfitting during the training, and the remaining 20,430 events for testing.

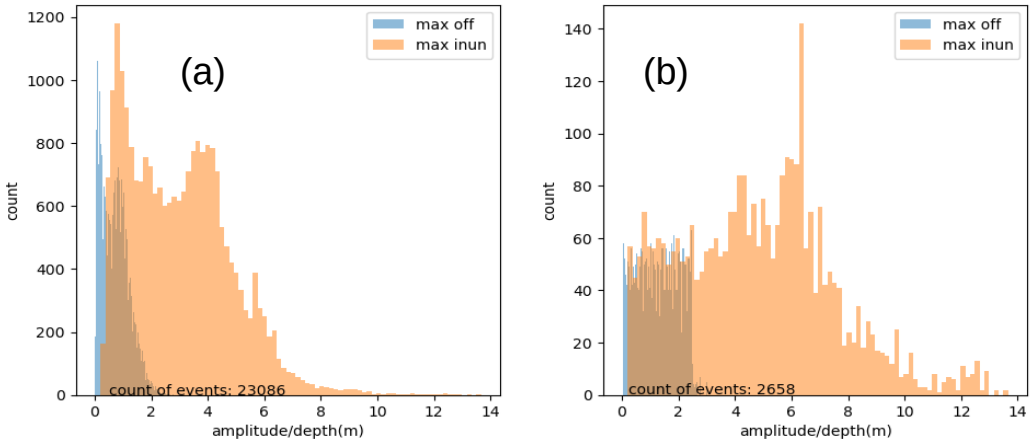

Figure 3. Histogram of the maximum offshore amplitude in blue at location 41 and the maximum inundation depth in orange across Catania for (a) the overall tsunami dataset (#23086 events) and (b) the training sample (#2655 events)

The training principle behind building an encoder-decoder is to minimise the reconstruction error between the input and the output of the decoder network using back propagation with mean squared error as the loss function. When such models are trained to reconstruct the input as output, they are called autoencoders(AE). We build our ML surrogate in two phases. In the first phase called pretraining, two autoencoder models with 64 latent variables are developed. One AE model is trained for the reconstruction of nine tsunami waveforms with dimensions 9 x 480. The second AE model is trained for the reconstruction of the maximum inundation depth at 416,318 locations which are prone to flooding based on the flood envelope across the training dataset, see Figure 5(c) for the location. In the second phase called fine tuning, the encoder from the first AE model (tsunami waveform) and the decoder of the second AE model (maximum inundation depth) are coupled using two dense interface layers to combine and fine-tune this final encoder-decoder style translation model shown in Figure 2.

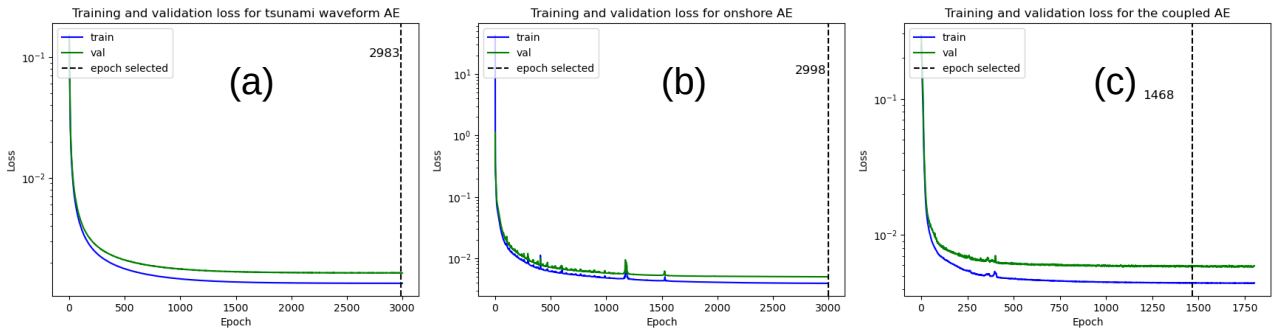

Figure 4. Model training and validation loss at different epochs across the three training phases: (a) pretraining the offshore AE for tsunami waveform, (b) pretraining the onshore AE for maximum inundation depth, (c) fine tuning a coupled model for translation of tsunami waveform to maximum inundation depth

The model parameters from the epoch having the least reconstruction error for both the training and validation set were selected for model prediction in the evaluation mode. The update of training weights was performed using a mini batch learning with a batch size of 300 for speed and efficiency and Adam optimizer for adaptive adjustment of the learning rates with early stopping, which prevents overfitting by stopping training if the model's performance does not improve for a certain number of epochs on the validation set.

3 Model prediction

We evaluate the model prediction by comparing the predicted maximum inundation depths from the model against the reference values from the tsunami simulation dataset. The model performs well in the overall characteristics like predicting the maximum inundation depth over the flood envelope (Fig. 6a) and the area inundated (Fig. 6d). There is an evident bias (overestimation of the flooded area) for smaller events where fewer than 1,000 pixels are inundated, i.e., about 0.1 km^2. The training dataset did not consider such small events and the focus of the performance evaluation is on the more significant tsunami flooding events. To see the prediction for a larger event, we plot the prediction and the misfit for event #1795 (Fig. 6b and 6c) which was selected based on the mean squared error (MSE) at the 99.9% quantile from our test set. It is among the 20 worst-predicted events in the test set.

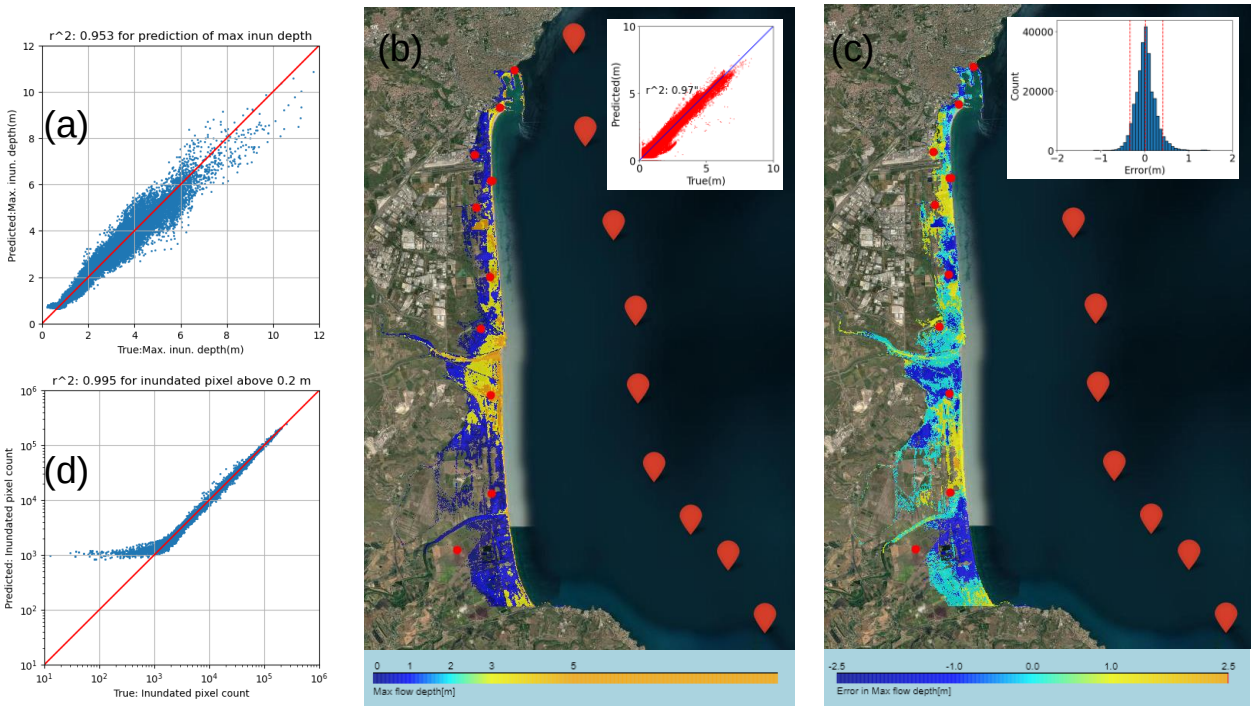

Figure 6. (a) Scatter plot between true and predicted values of the maximum inundation depth across the flood envelope for the test set. (b) Prediction of the maximum inundation depth for event #1795 whose prediction bias in terms of MSE metric for the test set MSE is above the 99.9% quantile. Red points mark 12 control points for evaluating the prediction. (c) Same as (b), with error in predicted depth for event #1795. (d) Scatter plot checking the fit between true and predicted inundated pixel count across the flood envelope for the test set.

At the 12 randomly selected control locations marked in Figure 6(b), we evaluate the misfit in terms of the error and coefficient of determination r^2, plotted with the scatter plot of the true and predicted value in Figure 7. Lastly, to assess the event level performance of our proposed models, we use the goodness-of-fit (G) statistic for each test event given by Equation 1, where T_i and P_i are the maximum inundation depth from the true (tsunami dataset) and predicted (model) at a location i of the N locations where T_i exceeds 0.2 m. Previous studies have used this statistic to compare the fit for waveforms and inundation depth (Lorito et al., 2008, Mulia et al., 2022).

$$G = 1 - 2\frac{\sum_{i=1}^{N} T_i P_i}{\sum_{i=1}^{N} {T_i}^2 + \sum_{i=1}^{N} {P_i}^2} \qquad (1)$$

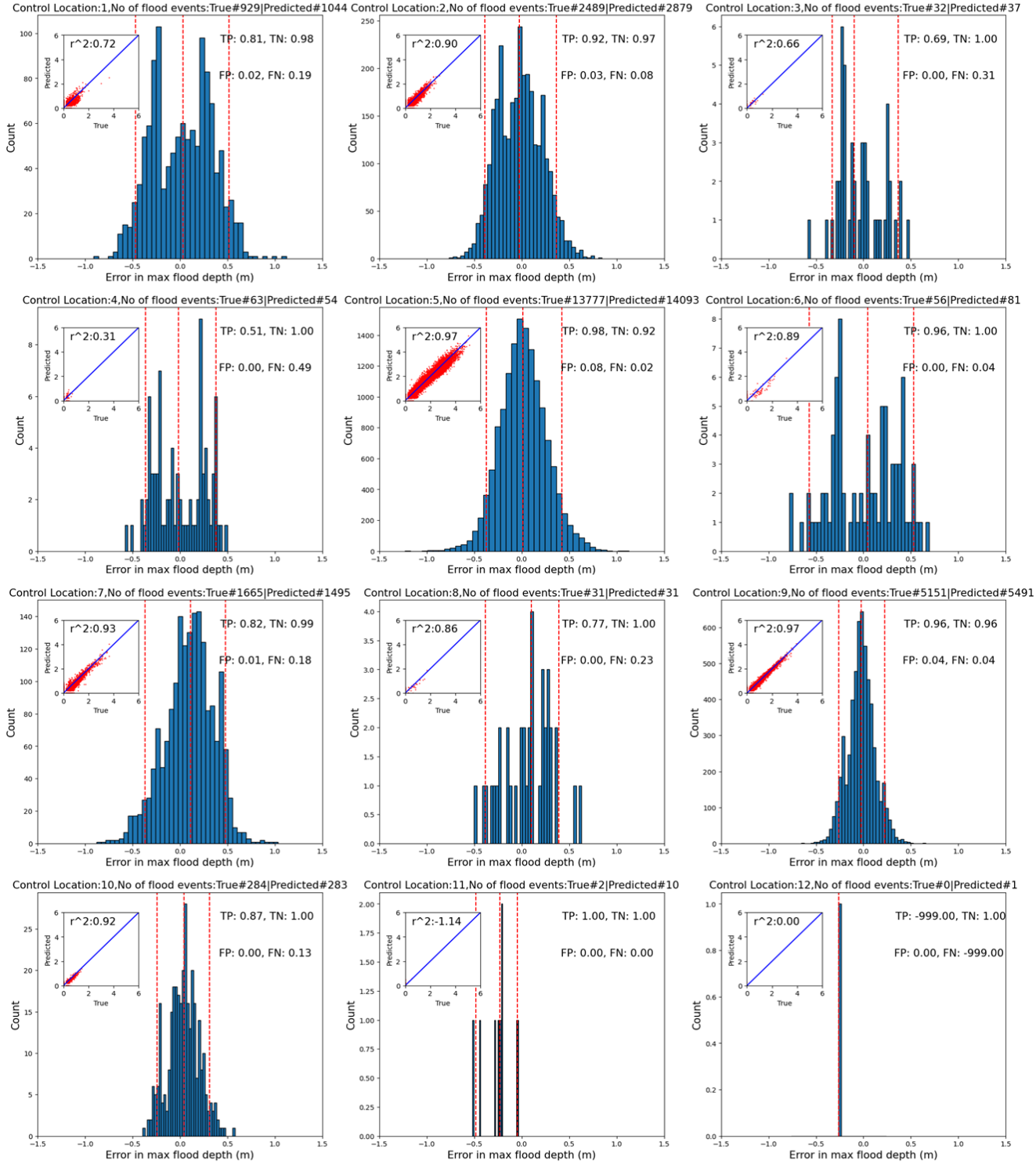

Figure 7. Evaluation of the misfit in prediction at the control locations in Figure 6b. In each inset is the scatter plot for that location of the true vs predicted values and coefficient of determination r^2.

Figure 8(a) shows the box plot for G across the different bins of the maximum wave amplitude recorded at location 41 offshore, to assess the variability in the performance of the model, and Figure 8(b) maps G at each event's earthquake epicentre (Fig 1c). The value of G ranges between 0-1, with a value closer to 0 representing good prediction accuracy.

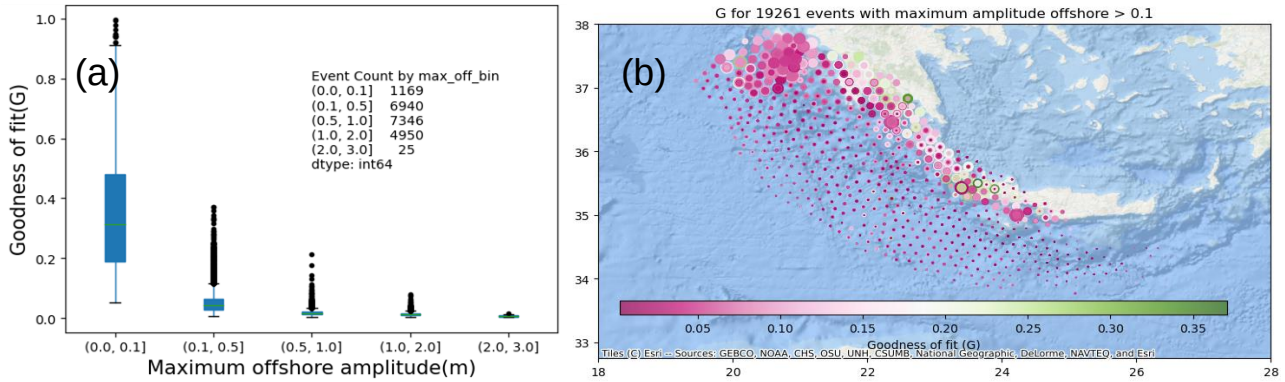

Figure 8. (a) Box plot showing the variability in the accuracy using G for different input wave amplitudes at location 41. (b) Map visualising the location of the earthquakes at the HSZ source region and the accuracy in prediction with G for all events with offshore maximum amplitude greater than 0.1 m

4 Rapid inundation and impact assessment

4.1 Population and settlements at risk

The prediction of the maximum inundation depth at a location, and related variables like the inundation area across the region of interest for an event, provide useful characteristics of the magnitude and the like severity of impact or damage. Incorporating information about the exposed population or built environment can help highlight and reduce the wide area at risk of tsunami flooding to regions most impacted. This provides additional characterization needed to prioritise resource allocation and response given the short lead time of such emergency and recovery activity.

To understand the impact on a local community in Catania, we use two products from the Global Human Settlement Layer (Schiavina et al 2023), the population count from GHS-POP-R2023A raster available at 100 m resolution and the settlement characteristics from GHS-BUILT-C R2023A raster available at 10 m resolution, as a proxy to the residential and non-residential built-up area. These exposure layers are disaggregated to the inundation locations at 10 m resolution.

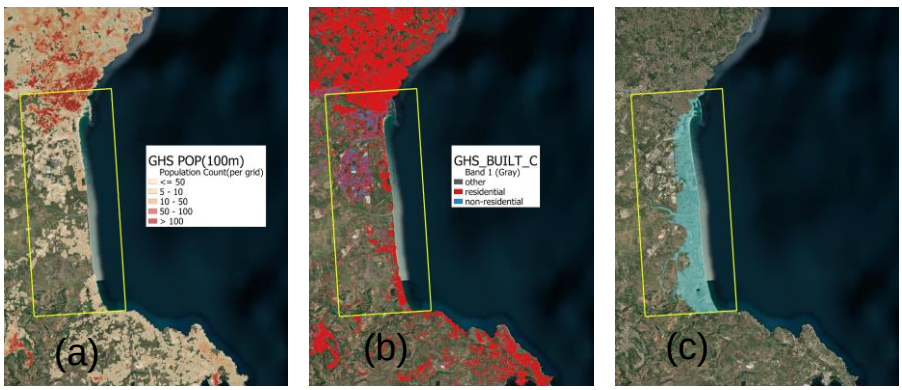

Figure 5. Different datasets to characterise the exposure in the built-up region of Catania (a) GHS POP (b) GHS built-up characteristics (c) Tsunami flood envelope where the exposure intersects with the inundation

Rapid assessment following a tsunami requires integrating multiple sources of information comprising hazard characteristics, community exposure and vulnerability, and provide ongoing updates as more information streams are available following an event. This could mean running multiple simulations of the tsunami model as the information on the earthquake sources keeps improving following the event or on the live tsunami sensor data at different time intervals.

4.2 Performance evaluation

To illustrate the reliability of the ML surrogate for such hazard characterisation, we summarise the accuracy of flood mapping at depth classes [0-0.2], [0.2-1], [1-3], [3-], which are based on the classification used for expected damage and actions to be taken for tsunami warning and advisories (JMA, 2023).

We verify the classification of the hazard or damage zones, concentrating on the populated grids of Catania, using the GHS-POP dataset for the model results for event #1795 from the synthetic catalogue as an example of rapid assessment. This helps assess the prediction at 254,367 populated locations of higher importance (out of the total 416,318 10-m prediction grids). These populated locations account for a population totalling 2,197 out of 4,262 people residing in the flood envelope (Fig 5c). Table 1 presents a confusion matrix summarizing the multi-class classification results detailing the true and predicted classification across the depth bins for event #1795 and the overall accuracy score given by Equation 2,

$$accuracy(y, \hat{y}) = \frac{1}{N}\sum_{i=1}^{N} \quad 1(\hat{y}_i = y_i) \qquad (2)$$

where $\hat{y}_i$ is the predicted class of the i-th location with y_i is the corresponding true class for N number of locations, with $1(x)$ representing the indicator function. The precision quantifies how accurately the model identifies instances of a class, given by the proportion of true positive predictions (correctly predicted positives) relative to all instances predicted as positive. The recall measures the sensitivity to map a particular class, given by the proportion of true positive predictions relative to all instances that are actually positive.

Table 1. Confusion matrix for calculating the accuracy of flood mapping for event #1795.

True depth class	**Predicted depth class**					
	[0-0.2]	[0.2-1]	[1-3]	[3-]	**Total**	**Recall**
[0-0.2]	54010	6166	65	0	60241	0.895
[0.2-1]	5167	35719	3902	0	44888	0.796
[1-3]	24	3762	71618	1794	77498	0.924
[3-]	0	1	752	10828	11581	0.936
Total	59201	45748	76037	2848		
Precision	0.911	0.781	0.94	0.791	**accuracy score: 0.888**	

We also check the performance of the model across the test events. The inundation depth values are used to map the affected population as safe, low, medium and high to sum as total impacted population and model the damage to the built-up area as no damage [0%], low [30%], medium [50%], completely destroyed or washed away [100%] to assess damage as total built area lost. The prediction accuracy for the affected population, and damaged built area for residential and non-residential occupancy is summarised in Figure 9.

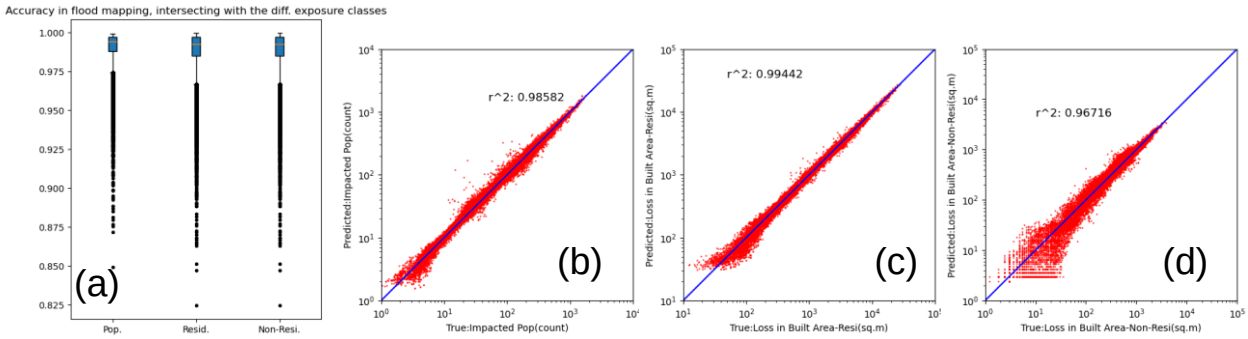

Figure 9. (a) Box plot showing the variability in the accuracy mapping the flood classes for different exposure grids – population, residential and non-residential. (b) Scatter plot comparing the true and predicted number of impacted people with the coefficient of determination r^2. (c) Same as panel (b) with loss of built area(residential). (d) Same as panel (b) with loss of built area(non-residential)

5 Discussion and conclusion

Reliable rapid hazard and damage assessment are necessary for informed decisions after natural disasters, especially a tsunami where a wide region may be affected. We show the application of a class of neural network models called encoder-decoders, which can be efficiently trained as a tsunami waveform translator to predict local-scale inundation with 10 m resolution, using the eastern coast of Sicily for the city of Catania as an example. The idea is similar to using a denoising autoencoder to predict tsunami waveforms nearshore based on the sparse inputs from an observation network, as proposed by Liu et al. (2022) but differs in the output. Here we predict the maximum inundation depth across a large number of locations which are needed for real-time and rapid post-event analysis. To have stable training and faster convergence, we use a two-part process of pre-training and fine tuning. This allowed us to train the model with just 1,939 events. We achieved a high accuracy rate with average goodness of fit (G) across a set of 20,340 test events having an average equal to 0.0493. The algorithm demonstrated its use for rapid inundation and impact assessment for test events, by verifying its high classification accuracy at different depth classes relevant to early warning and rapid assessment for three different open exposure distribution spreads – population, residential and non-residential. In rapid assessment where the source uncertainty needs to be explored, across the inundation hazard and expected losses, the model provides a fast and accurate solution.

The model proposed in its current form suffers from some simplification which needs to be addressed before real application. We only considered a single earthquake source zone, i.e., the Hellenic subduction zone (HSZ), for this study but the model will need to be trained with tsunami events across the Mediterranean region affecting the Catania region. Another limitation is that we do not consider the impact of local tidal conditions and the local co-seismic deformation on the inundation, which can significantly impact the inundation process. The vulnerability and exposure components of the risk analysis were conducted in a fairly simplified way to demonstrate the application of the ML surrogate. This can be improved by using fragility functions representative of the regional building classes and quality and local exposure relevant to the decision maker's needs, and by propagating the uncertainty. Further, an alternative approach is to train the model to directly predict risk metrics, bypassing the need for inundation predictions as intermediate inputs for subsequent risk calculations, as demonstrated by Li and Goda (2022). Through the use of a machine learning surrogate, it becomes feasible to directly map and predict metrics related to the impacted population, building damage, or losses.

6 References

Ahmed, S.M.S. and Güneyli, H. (2023) 'Automatic post-tsunami loss modelling using deep learning CNN case study: Miyagi and Fukushima Japan tsunami', Nat Hazards 117, 3371–3397 (2023). https://doi.org/10.1007/s11069-023-05991-2.

de la Asunción, M. et al. (2013) 'Efficient GPU implementation of a two waves TVD-WAF method for the two-dimensional one layer shallow water system on structured meshes', Computers & Fluids, 80, pp. 441–452. Available at: https://doi.org/10.1016/j.compfluid.2012.01.012.

Baba, T., Takahashi, N. and Kaneda, Y. (2014) 'Near-field tsunami amplification factors in the Kii Peninsula, Japan for Dense Oceanfloor Network for Earthquakes and Tsunamis (DONET)', Marine Geophysical Research, 35(3), pp. 319–325. Available at: https://doi.org/10.1007/s11001-013-9189-1.

Bai, Y. et al. (2018) 'A Framework of Rapid Regional Tsunami Damage Recognition From Post-event TerraSAR-X Imagery Using Deep Neural Networks', IEEE Geoscience and Remote Sensing Letters, 15(1), pp. 43–47. Available at: https://doi.org/10.1109/LGRS.2017.2772349.

Basili, R. et al. (2021) 'The Making of the NEAM Tsunami Hazard Model 2018 (NEAMTHM18)', Frontiers in Earth Science, 8. Available at: https://www.frontiersin.org/articles/10.3389/feart.2020.616594 (Accessed: 2 August 2022).

Chen, Y. and Ji, W. (2021) 'Rapid Damage Assessment Following Natural Disasters through Information Integration', Natural Hazards Review, 22(4), p. 04021043. Available at: https://doi.org/10.1061/(ASCE)NH.1527-6996.0000504.

Folch, A. et al. (2023) 'The EU Center of Excellence for Exascale in Solid Earth (ChEESE): Implementation, results, and roadmap for the second phase', Future Generation Computer Systems, 146, pp. 47–61. Available at: https://doi.org/10.1016/j.future.2023.04.006.

Fraser, S. et al. (2013) 'Tsunami damage to coastal defences and buildings in the March 11th 2011 Mw9.0 Great East Japan earthquake and tsunami', Bulletin of Earthquake Engineering, 11(1), pp. 205–239. Available at: https://doi.org/10.1007/s10518-012-9348-9.

Gibbons, S.J. et al. (2020) 'Probabilistic Tsunami Hazard Analysis: High Performance Computing for Massive Scale Inundation Simulations', Frontiers in Earth Science, 8. Available at: https://doi.org/10.3389/feart.2020.591549.

Gusman, A.R. et al. (2014) 'A methodology for near-field tsunami inundation forecasting: Application to the 2011 Tohoku tsunami', Journal of Geophysical Research: Solid Earth, 119(11), pp. 8186–8206. Available at: https://doi.org/10.1002/2014JB010958.

Igarashi, Y. et al. (2016) 'Maximum tsunami height prediction using pressure gauge data by a Gaussian process at Owase in the Kii Peninsula, Japan', Marine Geophysical Research, 37(4), pp. 361–370. Available at: https://doi.org/10.1007/s11001-016-9286-z.

Japan Meteorological Agency. (2023). Tsunami Information - Japan Meteorological Agency. Retrieved from https://www.data.jma.go.jp/eqev/data/en/guide/tsunamiinfo.html. JMA 2023.

Kosaka, N. et al. (2023) 'Decision-making support utilizing real-time tsunami inundation and damage forecast', International Journal of Disaster Risk Reduction, 94, p. 103807. Available at: https://doi.org/10.1016/j.ijdrr.2023.103807.

Li, Y. and Goda, K. (2022) 'Hazard and Risk-Based Tsunami Early Warning Algorithms for Ocean Bottom Sensor S-Net System in Tohoku, Japan, Using Sequential Multiple Linear Regression', Geosciences, 12(9), p. 350. Available at: https://doi.org/10.3390/geosciences12090350.

Liu, C.M. et al. (2021) 'Comparison of Machine Learning Approaches for Tsunami Forecasting from Sparse Observations', Pure and Applied Geophysics, 178(12), pp. 5129–5153. Available at: https://doi.org/10.1007/s00024-021-02841-9.

Lorito, S., Piatanesi, A. and Lomax, A. (2008) 'Rupture Process of the 18 April 1906 California Earthquake from Near-Field Tsunami Waveform Inversion', Bulletin of the Seismological Society of America, 98(2), pp. 832–845. Available at: https://doi.org/10.1785/0120060412.

Makinoshima, F. et al. (2021) 'Early forecasting of tsunami inundation from tsunami and geodetic observation data with convolutional neural networks', Nature Communications, 12(1), p. 2253. Available at: https://doi.org/10.1038/s41467-021-22348-0.

Molinari, I. et al. (2016) 'Fast evaluation of tsunami scenarios: uncertainty assessment for a Mediterranean Sea database', Natural Hazards and Earth System Sciences, 16(12), pp. 2593–2602. Available at: https://doi.org/10.5194/nhess-16-2593-2016.

Mori, N. et al. (2011) 'Survey of 2011 Tohoku earthquake tsunami inundation and run-up', Geophysical Research Letters, 38(7). Available at: https://doi.org/10.1029/2011GL049210.

Mulia, I.E. et al. (2022) 'Machine learning-based tsunami inundation prediction derived from offshore observations', Nature Communications, 13(1), p. 5489. Available at: https://doi.org/10.1038/s41467-022-33253-5.

Mulia, I.E. and Satake, K. (2020) 'Developments of Tsunami Observing Systems in Japan', Frontiers in Earth Science, 8. Available at: https://www.frontiersin.org/articles/10.3389/feart.2020.00145 (Accessed: 3 October 2023).

Núñez, J. et al. (2022) 'Discriminating the occurrence of inundation in tsunami early warning with one-dimensional convolutional neural networks', Scientific Reports, 12(1), p. 10321. Available at: https://doi.org/10.1038/s41598-022-13788-9.

Schiavina M., Freire S., Carioli A., MacManus K. (2023): GHS-POP R2023A - GHS population grid multitemporal (1975-2030).European Commission, Joint Research Centre (JRC)
PID: http://data.europa.eu/89h/2ff68a52-5b5b-4a22-8f40-c41da8332cfe, doi:10.2905/2FF68A52-5B5B-4A22-8F40-C41DA8332CFE

Titov, V.V. et al. (2005) 'Real-Time Tsunami Forecasting: Challenges and Solutions', Natural Hazards, 35(1), pp. 35–41. Available at: https://doi.org/10.1007/s11069-004-2403-3.

Tsunami Early Warning and Mitigation System in the North Eastern Atlantic, the Mediterranean and Connected Seas, NEAMTWS, Implementation Plan (Third Session of the Intergovernmental Coordination Group for the Tsunami Early Warning and Mitigation System in the North Eastern Atlantic, the Mediterranean and Connected Seas, NEAMTWS), IOC Technical Series No. 73. UNESCO 2007. (Electronic copy, English only)

Wang, Y. et al. (2023) 'Coastal tsunami prediction in Tohoku region, Japan, based on S-net observations using artificial neural network', Earth, Planets and Space, 75(1), p. 154. Available at: https://doi.org/10.1186/s40623-023-01912-6.